


Cite this: *RSC Adv.*, 2020, 10, 14374

# Green synthesis of CuO nanoparticles using *Lantana camara* flower extract and their potential catalytic activity towards the aza-Michael reaction†

Rakesh Chowdhury,<sup>a</sup> Aslam Khan<sup>b</sup> and Md. Harunar Rashid<sup>\*,a</sup>

Aza-Michael addition is one of the most exploited reactions in organic chemistry. It is regarded as one of the most popular and efficient methods for the creation of the carbon–nitrogen bond, which is a key feature of many bioactive molecules. Herein, we report the synthesis of CuO nanoparticles by an alkaline hydrolysis process in the presence of the flower extract of *Lantana camara*, an invasive weed, followed by calcination in air at 400 °C. Microscopic results indicated that the plant extract played an important role in the modulation of the size and shape of the product. In the presence of extract, porous CuO nanostructures are formed. While mostly aggregated rod-shaped CuO nanostructures are formed in the absence of extract. The products are pure and highly crystalline possessing the monoclinic phase. The CuO nanoparticles have been used as a catalyst in the aza-Michael addition reaction in aqueous medium under ultrasound vibration. The product yield is excellent and the catalyst is reusable up to the fifth cycle. The catalyst system can be extended to various substituted substrates with excellent to moderate yields.

Received 15th February 2020

Accepted 1st April 2020

DOI: 10.1039/d0ra01479f

rsc.li/rsc-advances

## 1. Introduction

Metal oxide nanomaterials prepared from earth-abundant and inexpensive metals have attracted considerable attention because of their prospect as viable alternatives to the expensive metal-based catalysts used in many conventional chemical processes.<sup>1</sup> Nanomaterials exhibit activities which are different from those of the corresponding bulk materials because of their size and shape-dependent physicochemical and optoelectronic properties.<sup>1,2</sup> The catalytic activity of nanomaterials represents a rich resource for chemical processes, employed both in industry and in academia.<sup>1</sup> The great interest in catalysis using nanomaterials has prompted the synthesis and investigation of a diverse range of highly functionalized nanoparticles (NPs), including metal oxide nanostructures.<sup>3–7</sup> Cu based nanomaterials which are cheap and environmentally friendly are especially attractive in this context due to the high abundance of Cu in nature and the available simple and straightforward techniques to synthesize these nanomaterials.<sup>8</sup> Also, Cu based materials can promote and undergo a variety of reactions due to the wide range of accessible oxidation states of Cu such as Cu(0), Cu(I), Cu(II), and Cu(III) which enable reactivity *via*

multiple pathways. Because of these distinctive properties, Cu based nanomaterials are widely used as catalysts in various organic transformations including electrocatalysis, and photocatalysis.<sup>9–14</sup> However, it is challenging to develop a synthesis method for Cu based nanocatalysts that are highly active, selective, stable, and robust.<sup>15</sup> Among various Cu based materials, copper oxide (CuO) is one of the simplest and industrially important semiconductor materials belonging to the monoclinic structure system with a narrow bandgap energy of 1.2 eV.<sup>16</sup> Because of the potential applications in various fields,<sup>8,17–19</sup> CuO nanostructures with various sizes and morphologies have been prepared *via* several methods such as sonochemical,<sup>20</sup> solvothermal,<sup>21</sup> hydrothermal,<sup>11</sup> thermal decompositions,<sup>22</sup> electrochemical<sup>15,23</sup> and sol-gel method.<sup>24,25</sup> However, the use of expensive and toxic chemicals in the form of either stabilizing or capping agent in most of these methods limits their use in a wider range as they are neither eco-friendly nor environment-friendly. In order to overcome this, another rapidly growing promising method that requires special mention has emerged recently which utilizes the plant-derived extracts serving as both shape-directing and/or capping agents. For instance, Kumar *et al.* used eco-friendly and non-toxic *Aloe vera* leaf extract to synthesize CuO NPs by treating copper acetate with the extract at 100–120 °C for 24 h.<sup>26</sup> The CuO NPs formed are in the monoclinic phase with a particle size of 20 nm. These CuO NPs showed excellent antibacterial activity against fish pathogens. Sankar *et al.* synthesized rod-shaped CuO NPs of mean particle size 140 nm by reacting cupric sulfate with *Carica papaya* leave extracts at room temperature.<sup>19</sup>

<sup>a</sup>Department of Chemistry, Rajiv Gandhi University, Rono Hills, Doimukh, 791 112, Arunachal Pradesh, India. E-mail: harunar.rashid@rgu.ac.in

<sup>b</sup>King Abdullah Institute for Nanotechnology, King Saud University, Riyadh 11451, Saudi Arabia

† Electronic supplementary information (ESI) available. See DOI: 10.1039/d0ra01479f



These CuO nanorods were used for photocatalytic degradation of dyes under sunlight. Nasrollahzadeh *et al.* reported the synthesis of CuO NPs by a biological method using aqueous extract of *Thymus vulgaris* L. leaves as a reducing and capping agent.<sup>27</sup> The green synthesized CuO NPs were found to be excellent heterogeneous catalysts for ligand-free *N*-arylation of indoles and amines. Jadhav *et al.* reported an easy green synthesis method of CuO and Ag–CuO NPs using *Malus domestica* leaf extract as a stabilizing agent.<sup>28</sup> The synthesized NPs are spherical and crystalline in nature with average sizes between 18 and 20 nm. The *Malus domestica* leaf-capped NPs exhibited interesting antibacterial activity with both Gram-positive and Gram-negative bacteria at microgram concentrations. Veisi *et al.* reported a biological procedure for the synthesis CuO NPs utilizing aqueous leaves extract of *Thymbra spicata* as a reducing and capping agent.<sup>29</sup> The synthesized CuO NPs was employed as an appropriate nanocatalyst for ligand-free *N*-arylation of indole and aniline via Ullmann-type C–N coupling reactions. A biogenic synthesis method of luminescent CuO NPs via peel extracts of *Musa acuminata* was reported by Chaudhary *et al.*<sup>30</sup> They employed the distinctive optical and luminescence properties for sensing application for heavy metal ions using spectrophotometric analysis method. Hekmati *et al.* prepared CuO NPs through a biological procedure using the *Rosa canina* fruit extract as a capping and reducing agent.<sup>31</sup> These CuO NPs were used as an effective heterogeneous nanocatalyst for the three-component reaction of amines, aldehydes and alkynes (A3 coupling) to obtain various propargyl amines in a good yield. However, most of the plants used so far for the synthesis of CuO NPs are commercially valuable. So, the use of such plants in nanomaterials synthesis sacrificing their commercial values is not an appropriate approach. Rather invasive weed is the best alternative which serves the same purpose. So, following our previous success on the use of invasive weed for the synthesis of metal and metal oxide nanomaterials,<sup>4,32–35</sup> we intend to report herein the synthesis of CuO NPs by using flower extract of invasive weed, *Lantana camara* plant as capping-cum-shape directing agent.

aza-Michael addition is one of the most exploited reactions in organic chemistry. It is regarded as one of the most popular and efficient methods for the creation of the carbon–nitrogen (C–N) bond, which is a key feature of many bioactive molecules.<sup>36</sup> Moreover, it is the shortest pathway to  $\beta$ -amino carbonyl compounds including  $\beta$ -amino acid derivatives, which are useful building blocks for the synthesis of biologically active molecules and some essential intermediates of antibiotics and pharmaceutical products.<sup>37</sup> Generally, aza-Michael addition proceeds in the presence of strong acids or bases with the production of some by-products.<sup>36,38</sup> Recently, many synthetic methods for preparing the  $\beta$ -amino carbonyl compounds have been reported using Lewis or Brønsted acids and transition metal salts to improve and modify this reaction.<sup>36,39–41</sup> However, many of them suffer from several drawbacks from economic, environmental, or synthetic viewpoints and deal often with only terminal alkenes. Thus, chemists have paid more attention to the development of milder catalytic systems. Consequently, a number of

Table 1 Reaction recipe for the synthesis of CuO NPs

Components	CuO-1	CuO-2	CuO-3	CuO-4
Flower extract (wt%)	1.00	0.50	0.25	0.00
Copper(II) acetate (M)	0.05	0.05	0.05	0.05
NaOH (M)	0.20	0.20	0.20	0.20
Size from XRD	9.80	7.08	9.60	8.80

homogeneous catalysts such as boric acid,<sup>42</sup> Pd(*N,N*-ppo)Cl<sub>2</sub>,<sup>43</sup> ionic liquids,<sup>44,45</sup> *etc.* have been reported for the aza-Michael reaction. However, the loss of material and difficulty of purification in each step of the reaction dramatically reduces the overall efficiency of a synthetic process. Thus, not only the catalytic activity and selectivity but also the stability and reusability for safe, non-toxic, sustainable chemistry and green organic synthesis, have become particular interests in the development of heterogeneous metal oxide catalysts. Therefore, the development of a perfect heterogeneous metal oxide catalyst that meets the reactivity, selectivity, broad applicability and reusability criteria of a perfect catalyst is highly desirable. In this context, a lot of heterogeneous catalysts based on supported metal salts or NPs were employed with good catalytic activity.<sup>46–48</sup> However, the report on the use of metal oxide nanocatalyst for such reaction is very limited.<sup>12,49–51</sup> The benefit of using metal oxide NPs as

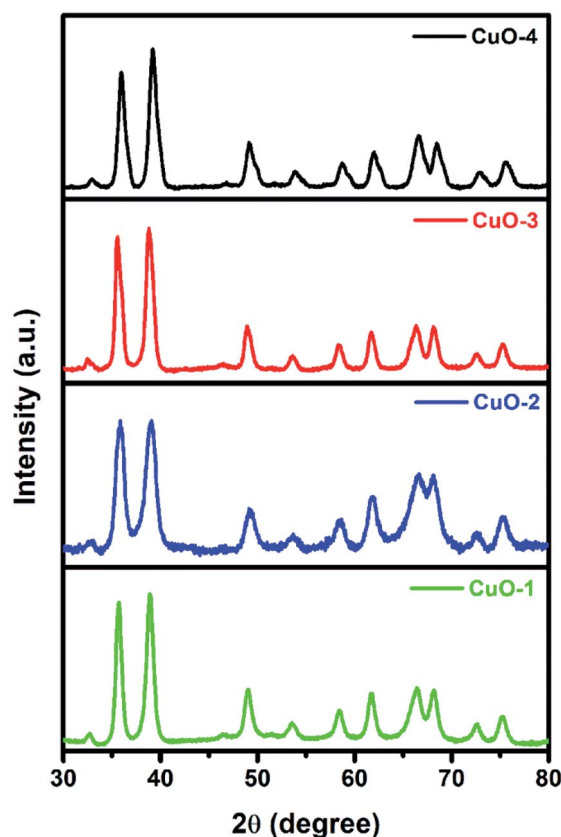


Fig. 1 X-ray diffraction pattern of different samples of CuO NPs.



catalyst such as high efficiency, enhanced surface to volume ratio, expected high atom economy, easy recovery and recyclability has prompted us to use the synthesized CuO NPs as catalyst for aza-Michael reaction.

## 2. Experimental section

### 2.1. Materials and methods

Flowers of the *Lantana camara* plant were collected from the Rajiv Gandhi University campus, Arunachal Pradesh, India. Copper(II) acetate monohydrate, sodium hydroxide pellets, ethanolamine, diaminoethane, aniline, and bulk CuO powder were purchased from Merck, India. Acrylonitrile, di-ethylamine, and all the substituted anilines were purchased from Sigma-Aldrich. All the chemicals were used without further purification and the required solutions for the synthesis of materials were prepared in double-distilled water. All the required glasswares were cleaned in a bath of aqua regia (1 : 3 HNO<sub>3</sub> and HCl) and then rinsed thoroughly with double distilled water.

### 2.2 Preparation of flower extract of *Lantana camara*

The phytochemicals were isolated from plant materials following our previously reported method.<sup>32</sup> The isolated dried mass was used to prepare a solution of 2.5 wt% extract in water.

### 2.3 Synthesis of CuO NPs

The synthesis of CuO NP involved a hydrolysis process using copper(II) acetate as a precursor and NaOH as the hydrolyzing agent in the presence of flower extract of *Lantana camara* plant. In a typical synthesis, copper(II) acetate solution (10 mL; 0.375 M), plant extract (30 mL; 2.5 wt%) and appropriate volume of water were mixed together in a stopper glass vessel under continuous stirring at 65 °C. After 10 minutes of stirring, 13 mL of NaOH solution (1.125 M) was added dropwise to raise the pH of the reaction mixture to 12. The reaction mixture was further heated at the same temperature under constant stirring for 2 h. After that, the reaction mixture was allowed to cool down to room temperature naturally. The product was isolated by centrifugation at 10 000 rpm for 10 min. The isolated product was then purified by two cycles of washing with water and centrifugation. Finally, the solid mass was dried in a vacuum oven at 60 °C for overnight. The dried product was subjected to calcination in a muffle furnace at 400 °C for 2 h to remove the hydroxyl ions or water molecules if any attached to the product. This set of reaction and the product is labeled as CuO-1. Following the same procedure similar set of reactions were carried out by varying the extract concentration to ascertain the role of extract either on the formation of CuO or on their size and shapes. The details of the reaction recipe are provided in

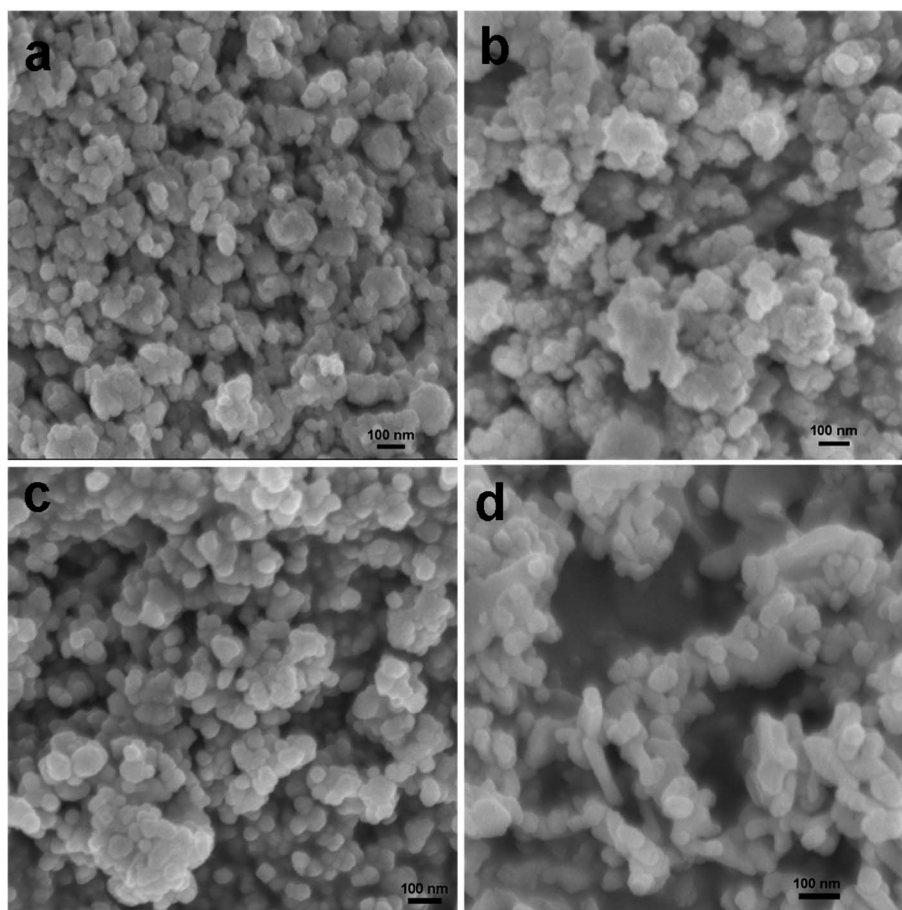


Fig. 2 SEM images of CuO NPs recorded from aqueous suspension of samples (a) CuO-1, (b) CuO-2, (c) CuO-3 and (d) CuO-4.





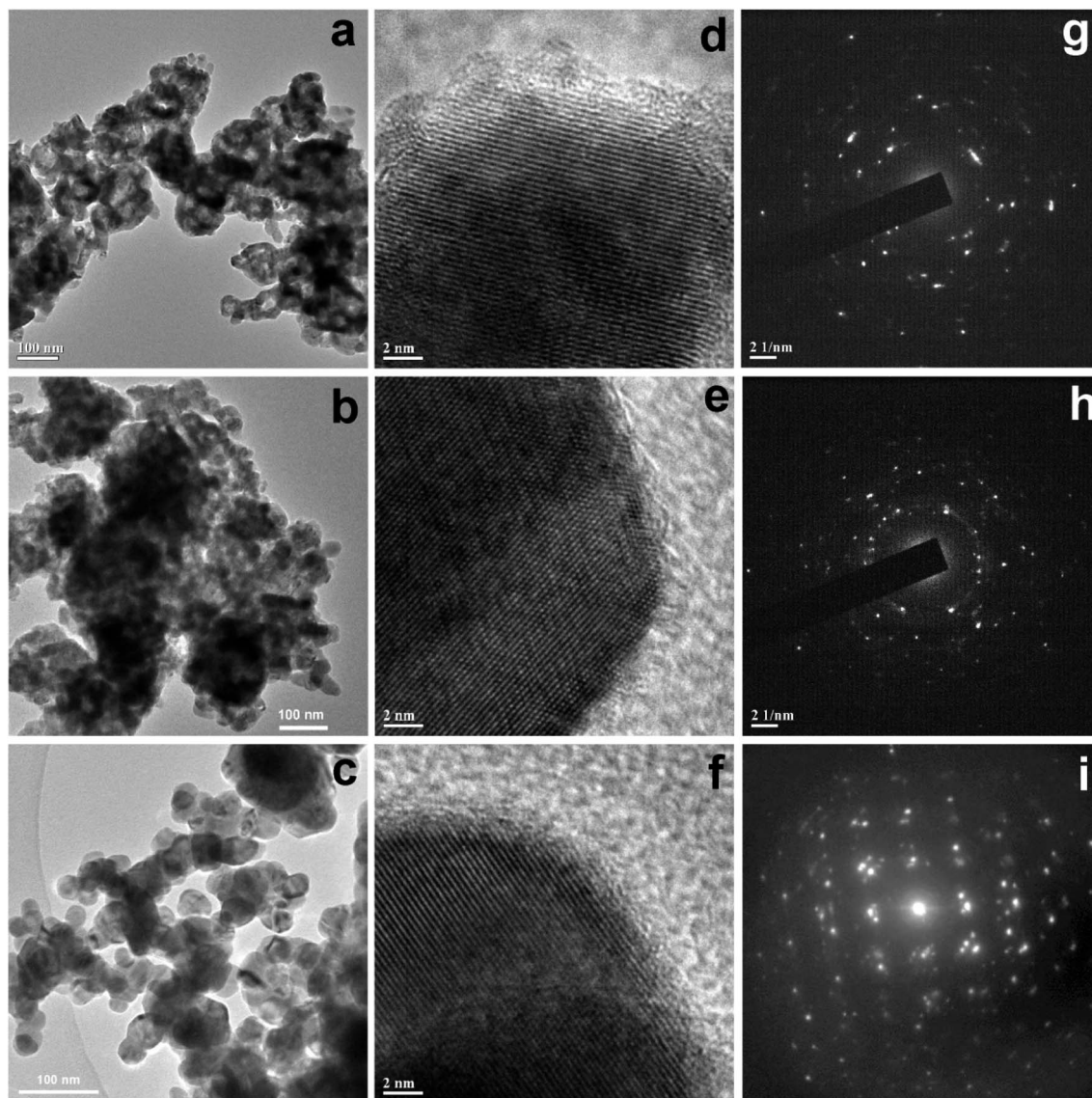


Fig. 3 TEM images of CuO NPs recorded from aqueous suspension of samples (a) CuO-1, (b) CuO-2, and (c) CuO-3. The respective HRTEM images and SAED patterns are shown in (d) and (g), (e) and (h) and (f) and (i) respectively for samples CuO-1, CuO-2, and CuO-3.

Table 1. All the synthesized materials were characterized by different spectroscopic, microscopic and diffractometric techniques. The details of the characterization techniques are provided in the ESI.†

#### 2.4 CuO catalyzed aza-Michael addition reaction

The catalytic activity of the synthesized CuO NPs was tested in aza-Michael addition reaction under ambient condition. For the initial investigation, we chose acrylonitrile (131  $\mu$ L; 2 mmol) and aniline (183  $\mu$ L; 2 mmol) as model substrates, and CuO (2 mg; 0.024 mmol) nanocatalyst under the solvent-free condition at room temperature. All substrates were mixed in a glass round bottom flask fitted with a reflux condenser and allowed to progress the reaction. The progress of the reaction was monitored by TLC. After completion of the reaction, the reaction mixture was extracted with ethyl acetate and water respectively.

The aqueous layer containing the catalyst was subjected to centrifugation at 12 000 rpm for 15 min to isolate the solid catalyst. The organic phase was then dried with  $\text{Na}_2\text{SO}_4$ , filtered, and the solvent was removed under reduced pressure. The crude product was purified by passing through a column of silica gel using ethyl acetate-*n*-hexane as the eluent. All products were known compounds, which were characterized by  $^1\text{H}$  and  $^{13}\text{C}$  NMR spectroscopy and their melting points (MPs) were compared with literature reports.

#### 2.5 Reuse of the CuO catalyst

To check the reusability of the catalyst, the isolated solid catalysts were purified by repeated washing with a mixture of ethyl acetate and water to get rid of any organic compounds and centrifugation and finally the isolated catalyst was dried at 60  $^\circ\text{C}$ . The dried catalyst was again used in a new batch of

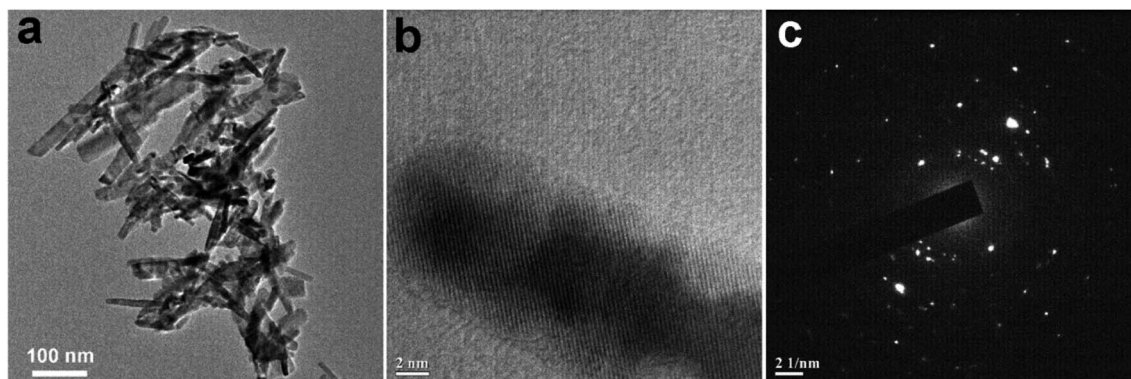


Fig. 4 (a) TEM images of CuO NPs recorded from an aqueous suspension of sample CuO-4 prepared in the absence of extract. (b) and (c) are the respective HRTEM image and SAED pattern recorded from sample CuO-4.

reaction taking the model reaction with substrates aniline and acrylonitrile.

### 3. Results and discussions

#### 3.1 X-ray diffraction study

The X-ray diffraction (XRD) study was undertaken to determine and to confirm the crystalline structure of synthesized CuO NPs. Fig. 1 shows the appearance of diffraction pattern at  $2\theta = 32.7$ , 35.8, 38.9, 49.0, 53.7, 58.5, 61.8, 66.3, 68.5, 72.6 and 75.4 which are assigned to the planes (110), (002)/( $\bar{1}11$ ), (111)/(200), ( $\bar{2}02$ ),

(020), (202), ( $\bar{1}13$ ), (311), (220), (311) and (004) respectively of monoclinic phase CuO (JCPDS file no.: 48-1548). No characteristic peak due to any impurity was observed in the diffractograms suggesting the formation of pure crystalline CuO. The average size of the CuO was calculated by using the Debye-Scherrer equation (eqn (1))<sup>52</sup> considering the diffraction peaks at  $2\theta = 38.9^\circ$ . The average crystallite size in the samples of CuO NPs is below 10 nm (Table 1).

$$D = \frac{0.9\lambda}{\beta \cos \theta} \quad (1)$$

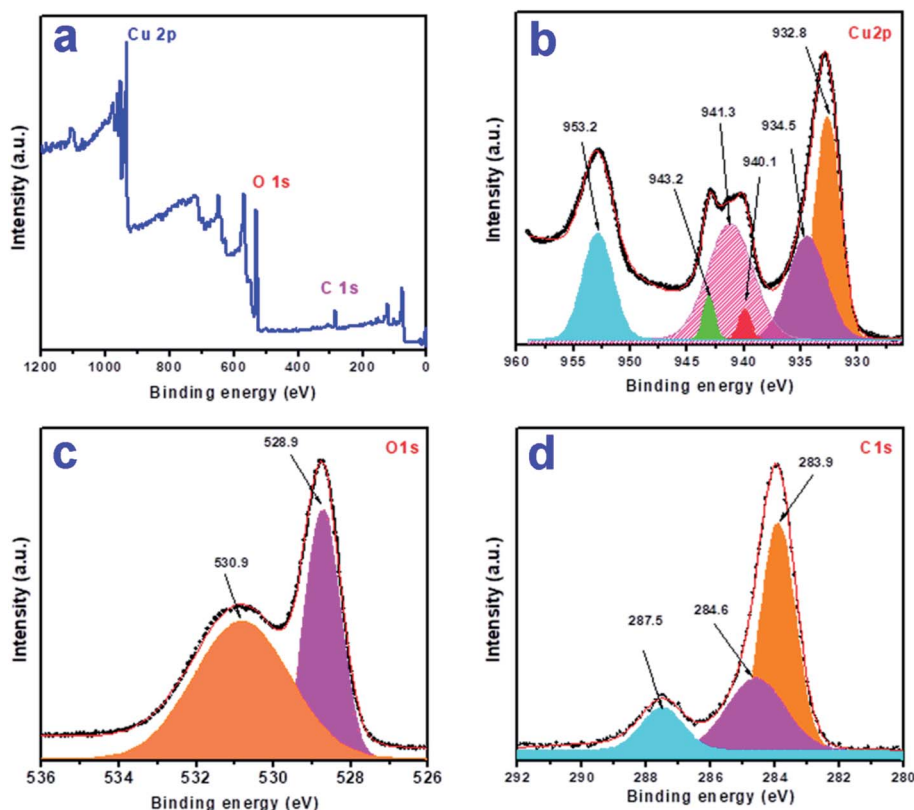


Fig. 5 X-ray photoelectron spectra of sample CuO-1: (a) survey scan, (b) Cu 2p, (c) O 1s and (d) C 1s region.



where  $\lambda$  is the wavelength of the X-ray radiation (0.154 nm),  $\theta$  is the diffraction angle and  $\beta$  is the full width at half maximum (FWHM).

### 3.2 Microscopic study

In order to confirm the surface topography and to study the morphological evolution of the products, we recorded the scanning electron microscopy (SEM) and transmission electron microscopy (TEM) images of all the samples. Fig. 2a shows the SEM images of the sample CuO-1 NPs, which is synthesized in the presence of 1.0 wt% plant extract. Spherical shape CuO nanoparticles were observed in the SEM image. It seems that the diameter of such CuO NPs ranges from 13 nm to 28 nm. When the plant extract concentration was reduced from 1.0 wt% to 0.5 wt% formation of spherical shape CuO NPs were observed in sample CuO-2 also (Fig. 2b). However, it seems that the sizes of the particles are larger than the previous sample. Further decrease in the plant extract concentration in sample CuO-3 again shows the formation of spherical CuO NPs (Fig. 2c). Visual observation of the images clearly indicates that the particle size in sample CuO-3 is larger than those of the previous two samples prepared with a higher concentration of the plant extract. The results clearly indicated that the phytochemicals present in the plant extract act not only as the stabilizer but also as capping agents which modulated the size of the formed CuO NPs during its growth. Further to investigate the role of plant extract, the SEM image of sample CuO-4 prepared without the addition of plant extract was recorded. Surprisingly formation of rod-shaped CuO NPs along with spherical particles could be observed in the SEM image (Fig. 2d). There is no uniformity in the size or shape of the particles in this sample implying that no proper control on growth took place in the absence of additive. So, it is obvious that plant extract act as a capping agent in the formation of CuO NPs.

Further TEM images of all the samples were recorded to investigate the morphological evolution. The TEM image of sample CuO-1 (Fig. 3a) shows the presence of smaller sized spherical CuO NPs which are assembled in a particular fashion to form some larger sized spheres of sizes about 125 nm. As can be seen, there are voids within these spherical structures. The diameter of the smaller sized spherical particles measured from the isolated particles is in the ranges from 15 to 23 nm. In the case of sample CuO-2, nearly similar morphologies were observed (Fig. 3b) but the aggregation pattern is a little bit different compared to sample CuO-1. Also, the diameter of smaller sized particles constituting the larger structures is in the ranges of 20 to 30 nm. The TEM image of sample CuO-3 prepared with the lowest concentration of plant extract is dominated by mostly isolated spherical CuO NPs (Fig. 3c). The diameter of such nanoparticles is varied from 25 to 40 nm. This clearly indicated that a higher concentration of plant extract restricts the growth of particles during its formation and the presence of phytochemicals mainly composed of sugars, phospholipids, glycolipids, alkaloids, phenolics, tannins, *etc.*<sup>35</sup> assisted the particles to get aggregation in a particular orientation to form sponge-like structures. On the other hand, an

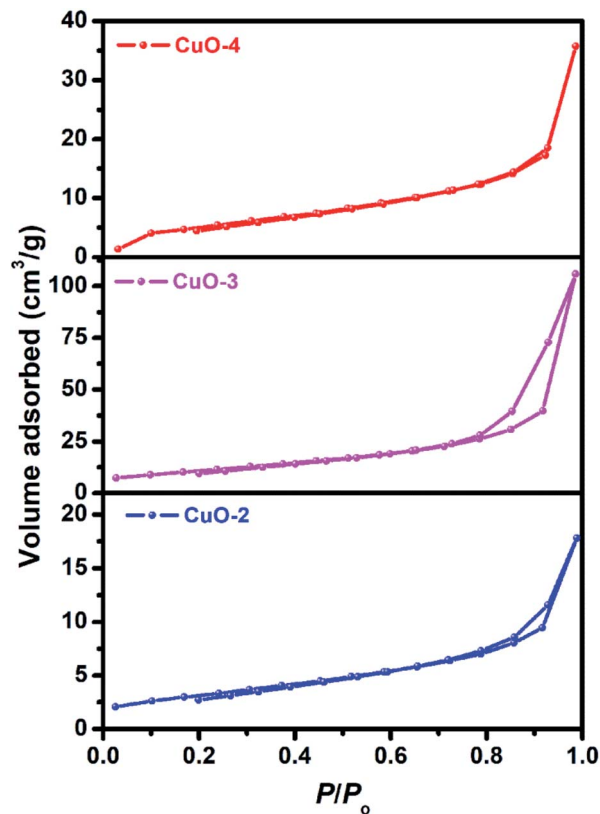


Fig. 6 Nitrogen gas adsorption-desorption isotherms of different samples of CuO nanostructures.

inadequate amount of plant extracts results in the formation of isolated spherical CuO NPs. In the absence of plant extract, the growth of particles is not well controlled resulting in the formation of rod-shaped CuO nanostructures of varying lengths and width in sample CuO-4 (Fig. 4a). It may be mentioned that the size of CuO NPs calculated from the XRD study is different from those observed in TEM and SEM study. The possible reason is that, TEM or SEM measures the particle size, whereas with XRD one can measure the crystallite size which is the coherent diffracting crystalline domains (crystallite) that is different from the particle size. One particle can be constituted by several crystalline domains (crystallites) and that is why the particle size is always bigger than crystallite size.

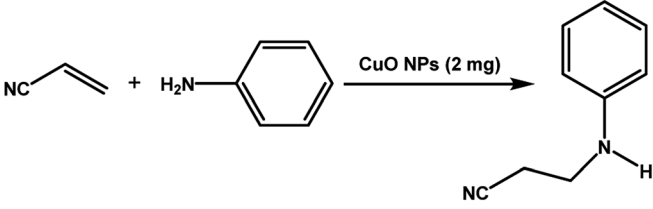
In order to understand the growth habits and crystalline properties of the products high-resolution TEM (HRTEM) images and the selected area electron diffraction (SAED)

Table 2 Specific surface area and pore characteristics of the as-prepared CuO nanostructures

Sample	Surface area (m <sup>2</sup> g <sup>-1</sup> )	Pore diameter (nm)	Pore volume (cm <sup>3</sup> g <sup>-1</sup> )
CuO-2	11.35	2.56	0.028
CuO-3	39.35	2.56	0.167
CuO-4	19.48	2.19	0.056





**Table 3** Optimization of the reaction condition for aza-Michael reaction<sup>a</sup>


Entry	Solvent	Temperature	Time (h)	Yield (%) <sup>b</sup>
1	Solvent-free	RT	24	30
2	Solvent-free	60 °C	9	50
3	Water	60 °C	9	70
4	Water + ethanol	60 °C	9	70
5	Ethanol	60 °C	9	65
6	Acetonitrile	60 °C	9	30

<sup>a</sup> Reaction condition: acrylonitrile = 2 mmol and aniline = 2 mmol.<sup>b</sup> Isolated yield.

patterns of the samples were recorded. Well resolved lattice fringes in the HRTEM images confirmed the formation of highly crystalline CuO NPs (Fig. 3d–f). The interplane space values as measured from the HRTEM images are 0.280, 0.264 and 0.283 nm for samples CuO-1, CuO-2 and CuO-3 respectively which correspond to (110), (002)/(111) and (110) lattice planes in CuO. The interplane space values for rods (Fig. 4b) was measured to be 0.254 nm corresponding to (002)/(111) lattice plane. The SAED patterns of all the samples (Fig. 3g–i) are dominated by bright spots superimposed on ring patterns confirming the presence of polycrystalline particles with the

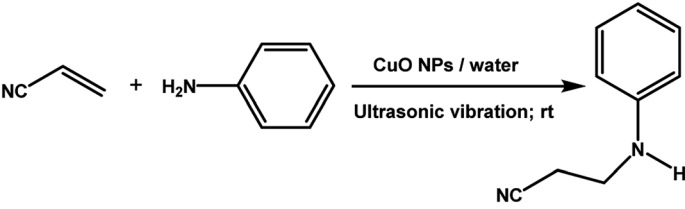
presence of some defects on their surfaces. A similar observation was also observed for sample CuO-4 (Fig. 4c).

### 3.3 X-ray photoelectron spectroscopy study

To know the elemental composition and the oxidation states of the elements present in the synthesized product, we analyzed the sample CuO-1 by X-ray photoelectron spectroscopy (XPS). A typical survey scan XPS spectrum of sample CuO-1 (Fig. 5a) shows the presence of elements C 1s, O 1s, and Cu 2p. The high-resolution XPS spectrum of Cu 2p region (Fig. 5b) shows the peaks at a binding energy of 932.8 eV and 953.2 eV which are attributed to Cu 2p<sub>3/2</sub> and Cu 2p<sub>1/2</sub> respectively.<sup>53</sup> The energy gap between the peaks Cu 2p<sub>1/2</sub> and Cu 2p<sub>3/2</sub> is 20.4 eV, which is very close to the standard value of Cu 2p in CuO. Besides, two shake-up satellites due to Cu<sup>2+</sup> are observed at 940.1 eV and 943.2 eV. These results confirm the presence of Cu<sup>2+</sup> state in the products ruling out the possibility of the presence of Cu<sub>2</sub>O phase.<sup>53</sup> Fig. 5c shows the O 1s core-level spectrum, where two peaks were observed in the fitted curve, one at 528.9 eV and another one at 530.9 eV. The peak found at 528.9 eV is due to O<sup>2-</sup> in CuO crystal lattice.<sup>54</sup> Whereas the peak at 530.9 is due to the chemisorbed oxygen associated with the surface adsorbed hydroxyl groups.<sup>54</sup> The results confirmed that the composition of the sample is CuO. Fig. 5d shows the fitted curve for the C 1s region which exhibits peaks at 283.9, 284.6 and 287.5 eV, which are due to the presence of C–C and C–O bonds respectively. The peaks are associated with either the adventitious carbon contamination or the chemisorbed carbon from the plant extract during the calcination process.

### 3.4 Study of the surface properties

To study the surface characteristics, Brunauer–Emmett–Teller (BET) surface area analysis was performed on the samples

**Table 4** Optimization of the catalyst loading for aza-Michael reaction under ultrasonic vibration<sup>a</sup>


Entry	Catalyst	Amount (mmol)	Time (h)	Yield% <sup>b</sup>
1	CuO-2	0.012	4	70
2	CuO-2	0.024	4	80
3	CuO-2	0.036	4	80
4	CuO-2	0.060	4	80
5	CuO-1	0.024	4	80
6	CuO-3	0.024	4	75
7	CuO-4	0.024	4	65
8	Bulk CuO	0.024	4	40
9	No catalyst	—	4	~30

<sup>a</sup> Reaction condition: acrylonitrile = 2 mmol and aniline = 2 mmol. <sup>b</sup> Isolated yield.

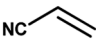
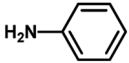
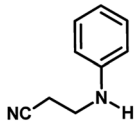
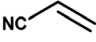
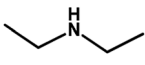
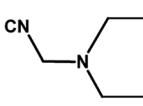
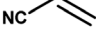

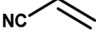
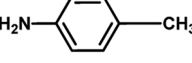
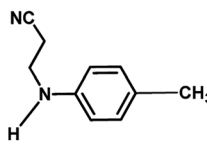
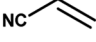
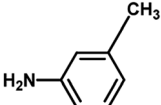
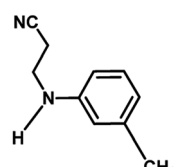
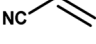
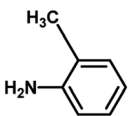
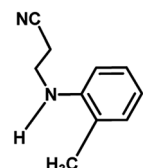
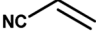
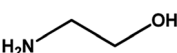
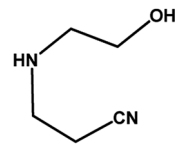
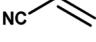
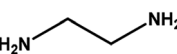
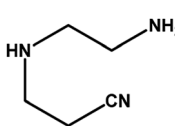
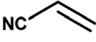
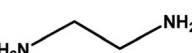
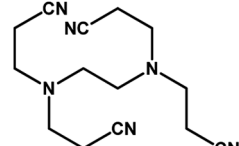
(Fig. 6). All the samples (sample CuO-2, CuO-3 and CuO-4) exhibited type H3 hysteresis with loop associated with aggregates of particles giving rise to narrow slit-like pores.<sup>55</sup> The surface parameters calculated from BET measurements of these samples are summarized in Table 2. It is clear from Table 2 that sample CuO-3 possesses very high surface area compared to sample CuO-2 and CuO-4. It might be attributed either to the different types of aggregated structures or morphology observed in different samples. Also, pore diameter and pore volume in

sample CuO-3 is much higher than sample CuO-4 but the pore diameters of samples CuO-2 and CuO-3 are same.

### 3.5 CuO catalyzed aza-Michael addition reaction

The catalytic activity of the synthesized CuO NPs (sample CuO-2) was tested in aza-Michael addition reaction under safe and eco-friendly reaction conditions. For the initial investigation, we chose acrylonitrile (2 mmol) and aniline (2 mmol) as model substrates and CuO (2 mg; 0.024 mmol) as nanocatalyst under

**Table 5** Substrate scope for the aza-Michael reaction under ultrasonic vibration (catalyst used = 0.024 mmol; solvent: water)

Entry	Substrate A (2 mmol)	Substrate B (2 mmol)	Product	Time	% yield
1				4 h	80%
2				30 min	90%
3			No product	4 h	X
4				4 h	85%
5				4 h	40%
6				4 h	20%
7				4 h	40%
8				4 h	55%
9				4 h	68%





the solvent-free condition at room temperature (Table 3, entry 1). Approximately 30% yield was observed after 24 h of reaction. To check if the performance of the catalyst can be improved at a higher temperature, the reaction temperature was raised to 60 °C keeping all other reaction conditions identical. We surprised to observe a significant increase in the yield up to 50% after 9 h. Further to check if the addition of solvent has any impact on the yield, we repeated the reaction at 60 °C in the various solvent environments, *e.g.* water, a mixture of water and ethanol, ethanol and acetonitrile keeping all other conditions identical (Table 3; entry 3–6). The highest yield (70%) was observed with water and water–ethanol mixed solvent system and so the water was chosen as the solvent system for further study considering its environment-friendly nature. Consideration of water as solvent also helps in obtaining a good dispersion of catalyst making the separation of the catalyst from the reaction mixture easy. Although the results are quite satisfactory, the energy consumption is the subject of concern in this reaction condition. In an attempt to minimize the energy consumption, we repeated the reaction in water under ultrasonic vibration at room temperature. To our delight, the reaction completed within a shorter reaction time (4 h) with 80% of isolated yield. Inspired by this satisfactory result, in the next assessment, we tried to optimize the amount of catalyst required for the reaction (Table 4). So, we repeated the reaction by varying the catalyst loading from 1 mg (0.012 mmol) to 5 mg (0.06 mmol). We observed 70% yields with 0.012 mmol of the catalyst whereas 0.024 mmol, 0.036 mmol and 0.06 mmol of catalyst produce 80% yield (Table 4). This implies that 0.024 mmol of the catalyst is enough for the required transformation if the other reaction conditions are kept identical. So, we fixed 2 mmol of acrylonitrile, 2 mmol of aniline and 0.024 mmol CuO as the catalyst under the ultrasonic condition at room temperature as the optimized condition for the desired transformation. Further to assess the effect of shape and size of the catalyst on the reaction rate, we repeated the reaction with the same amount of CuO NPs synthesized under different reaction conditions (Table 4; entry 5–7). Surprisingly, we observed that the catalytic activity of rod-shaped CuO NPs prepared in absence of the plant extract (sample CuO-4) is lower than that of the reaction catalyzed by spherical CuO NPs (sample CuO-2). Further, when the aza-Michael reaction was carried out in presence of bulk CuO under the optimized reaction condition, 40% product yield was recorded. It may be mentioned that in the absence of any catalyst, aza-Michael reaction yielded just 30% product under similar reaction condition. It is known that catalysis performance is a consequence of a sum of factors such as material characteristics and operational conditions and it is difficult to associate the activity just to one factor. It is believed that the surface area of a catalyst is one of the important parameter affecting the catalytic activity. But in the current study the catalytic activity is not dependent on the BET surface area. It was observed that CuO-3 possesses the highest surface area whereas CuO-2 possessed the least (Table 2). However, the catalytic activity of CuO-2 is very high compared to the other samples. One reason might be the presence of microporosity which restricts the diffusion of the

reactive species to the active sites. Another reason for lower catalytic activity of sample CuO-4 might be attributed to the aggregation of CuO crystallites due to absence of additive and hence the lower accessibility of the pores of CuO. Conclusively, we can say that BET surface area may not all be occupied by active surface sites and so it is difficult to say that active surface sites are proportional to BET surface area in the present study. But it is very clear from Tables 1 and 4 that CuO NPs prepared with higher amount of additive (1.0 and 0.5 wt%) exhibits higher catalytic activity. As the additive concentration decreases, the catalytic activity also decreases. CuO NPs prepared in the absence of additive showed the lowest catalytic activity. This clearly indicates that surface capping is important and the surface adsorbed species played a crucial role in modulating the catalytic activities of CuO NPs. However, the exact reason for the discrepancy in catalytic activity is not understood at this moment and hence need a detail study which is underway.

With the optimized reaction condition in hand, the generality of the newly developed protocol was expanded to a wide array of substituted aniline with electron-withdrawing and electron-donating groups at the *ortho*, *meta* and *para* positions as well as to aliphatic amines (Table 5). The yield with the substituted amine and aliphatic amines were found to be moderate to excellent. During substrate study, it was observed that the reaction of responsive group functionalized aniline underwent conversion easily to the corresponding products with high chemoselectivity (Table 5). That is a strong electron withdrawing groups like  $-\text{Cl}$  inhibit the reaction to occur (Table 5; entry 3) and the electron-donating groups such as  $-\text{CH}_3$  (Table 5; entry 4) increase the yield of the reaction. But the bulky effect dominates the reaction when they are present at *-ortho* and *-meta* position (Table 5; entry 5 and 6) and this effect leads to a remarkable decrease in the % yield of the conversion.

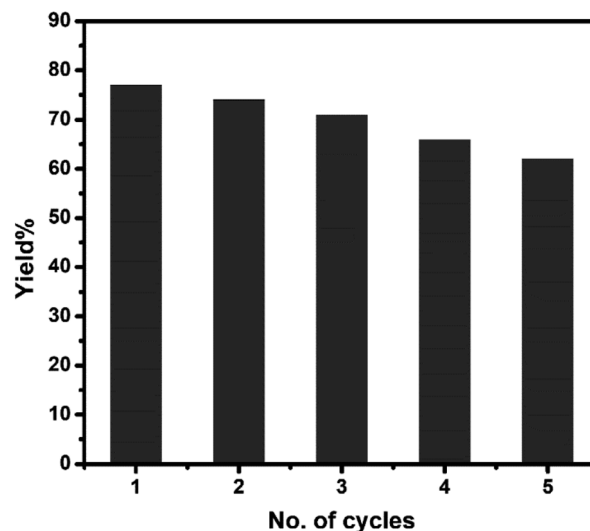


Fig. 7 Bar diagram showing the yield% of the product in different cycles of reuse of CuO nanocatalyst (sample CuO-2).



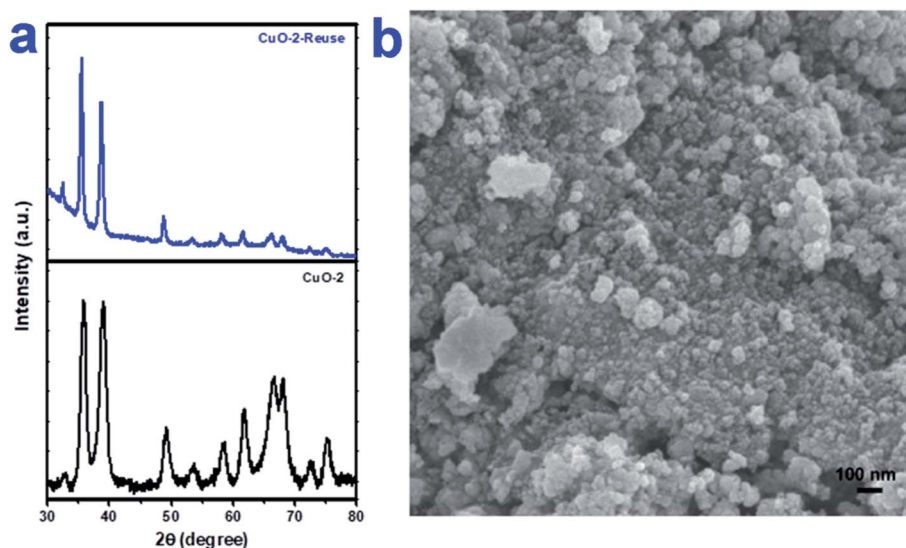


Fig. 8 (a) XRD pattern of CuO NPs (sample CuO-2) before and after use as catalyst in aza-Michael reaction and (b) the respective SEM image of CuO NPs (sample CuO-2) after use in catalysis.

### 3.6 Reusability of CuO nanocatalyst in aza-Michael addition reaction

To check the reusability of the catalyst, first, we separated the aqueous layer containing the catalyst after the reaction and isolated the products by centrifugation followed by repeated washing with water and water-ethanol mixture to get rid of any organic reactants or product. The isolated mass was dried in an oven at 60 °C under vacuum overnight. The isolated catalyst was used for new batches of aza-Michael reaction under identical reaction conditions as discussed above. The process was repeated for 5 cycles of reactions. The performance of the reused catalyst was quite satisfactory up to 5th cycles after which the efficiency of the catalyst decreased gradually (Fig. 7). The possible reason for the decrease in efficiency are-(i) some portion of the catalyst might undergo leaching during separation and purification of the catalyst and (ii) either the reactant or the products might undergo adsorption on the surface of the catalyst thereby deactivating the surface activity of the catalyst. To check the fate of the catalyst after the catalysis reaction, the isolated catalyst after use was analyzed by XRD and SEM. The comparison of the XRD pattern of sample CuO-2 (Fig. 8a) before and after analysis clearly indicated that the phase structure remains intact after catalysis. However, some XRD peaks of CuO-2-reuse are much weaker than those of CuO-2. The possible reason is that the amount of recovered sample used for XRD analysis was too little compared to the original sample. As a result diffraction intensity is diminished for some peaks. Also, there might be some disturbances in the crystalline properties due to catalysis. The respective SEM image (Fig. 8b) also supports that no morphological change took place during catalysis but we cannot deny the possibility of aggregation of the particles due to catalysis.

## 4. Conclusion

In summary, CuO nanoparticles (NPs) of different sizes and shapes were synthesized by precipitation method followed calcination of the product at 400 °C for 2 h in air. Flower extract of *Lantana camara* plant played the role of capping cum shape-directing agent to control the size and shape of the products. The synthesized CuO NPs are highly crystalline and are free from any impurities. The as-synthesized CuO NPs exhibits excellent catalytic activity towards the aza-Michael reaction of acrylonitrile with primary and secondary aliphatic and aromatic amines under ultrasonic vibration condition. CuO being non-toxic materials provides a greener pathway to produce a variety of substituted aza-Michael products. Also, CuO NPs are highly stable and can be reused for successive batches of reaction (up to 5<sup>th</sup> cycles) without much losing its catalytic activity.

## Conflicts of interest

The authors declare no conflict of interest.

## Acknowledgements

M. H. R. acknowledges Council of Scientific and Industrial Research, India (grant no. 01(2910)/17/EMR-II) for partially supporting the research. R. C. acknowledges Department of Science and Technology, India for providing the research fellowship (reg. no. IF150609). A. K. thanks the Researchers Supporting Project (RSP-2019/127), King Saud University, Riyadh, Saudi Arabia, for the financial support. The authors also thank SAIF, NEHU, NEIST, Jorhat and MARC, Bangalore for extending instrumental facilities to us.

## References

- 1 F. Zaera, Nanostructured materials for applications in heterogeneous catalysis, *Chem. Soc. Rev.*, 2013, **42**, 2746–2762.
- 2 L. L. Chng, N. Erathodiyil and J. Y. Ying, Nanostructured catalysts for organic transformations, *Acc. Chem. Res.*, 2013, **46**, 1825–1837.
- 3 A. T. Bell, The impact of nanoscience on heterogeneous catalysis, *Science*, 2003, **299**, 1688–1691.
- 4 S. Phukan, A. Mahanta and M. H. Rashid, Size-tunable ZnO nanotapes as an efficient catalyst for oxidative chemoselective C–B bond cleavage of arylboronic acids, *Appl. Catal., A*, 2018, **562**, 58–66.
- 5 S. Ostovar, D. Rodríguez-Padrón, F. Saberi, A. M. Balu and R. Luque, Versatile sulfathiazole-functionalized magnetic nanoparticles as catalyst in oxidation and alkylation reactions, *Catalysts*, 2019, **9**, 348.
- 6 N. S. Kumar, M. S. Reddy, V. R. Bheeram, S. B. Mukkamala, L. R. Chowhan and L. C. Rao, Zinc oxide nanoparticles as efficient catalyst for the synthesis of novel di-spiroindolizidine bisoxindoles in aqueous medium, *Environ. Chem. Lett.*, 2019, **17**, 455–464.
- 7 M.-S. Hosseini and M. Masteri-Farahani, Surface functionalization of magnetite nanoparticles with sulfonic acid and heteropoly acid: efficient magnetically recoverable solid acid catalysts, *Chem.-Asian J.*, 2019, **14**, 1076–1083.
- 8 M. B. Gawande, A. Goswami, F.-X. Felpin, T. Asefa, X. Huang, R. Silva, X. Zou, R. Zboril and R. S. Varma, Cu and Cu-based nanoparticles: synthesis and applications in catalysis, *Chem. Rev.*, 2016, **116**, 3722–3811.
- 9 K. Pan, H. Ming, H. Yu, Y. Liu, Z. Kang, H. Zhang and S.-T. Lee, Different copper oxide nanostructures: synthesis, characterization, and application for C–N cross-coupling catalysis, *Cryst. Res. Technol.*, 2011, **46**, 1167–1174.
- 10 R. Poreddy, C. Engelbrekt and A. Riisager, Copper oxide as efficient catalyst for oxidative dehydrogenation of alcohols with air, *Catal. Sci. Technol.*, 2015, **5**, 2467–2477.
- 11 P. Vinothkumar, C. Manoharan, B. Shanmugapriya and M. Bououdina, Effect of reaction time on structural, morphological, optical and photocatalytic properties of copper oxide (CuO) nanostructures, *J. Mater. Sci.: Mater. Electron.*, 2019, **30**, 6249–6262.
- 12 M. L. Kantam, S. Laha, J. Yadav and S. Jha, Nanocrystalline copper(II) oxide catalyzed aza-Michael reaction and insertion of  $\alpha$ -diazo compounds into N–H bonds of amines, *Tetrahedron Lett.*, 2009, **50**, 4467–4469.
- 13 Q. Zhou, T.-T. Li, W. Xu, H.-L. Zhu and Y.-Q. Zheng, Ultrathin nanosheets-assembled CuO flowers for highly efficient electrocatalytic water oxidation, *J. Mater. Sci.*, 2018, **53**, 8141–8150.
- 14 L. Mi, W. Wei, Z. Zheng, Y. Gao, Y. Liu, W. Chen and X. Guan, Tunable properties induced by ion exchange in multilayer intertwined CuS microflowers with hierarchal structures, *Nanoscale*, 2013, **5**, 6589–6598.
- 15 G. A. Somorjai and J. Y. Park, Molecular factors of catalytic selectivity, *Angew. Chem., Int. Ed.*, 2008, **47**, 9212–9228.
- 16 K. Borgohain, J. B. Singh, M. V. Rama Rao, T. Shripathi and S. Mahamuni, Quantum size effects in CuO nanoparticles, *Phys. Rev. B*, 2000, **61**, 11093–11096.
- 17 M. Karami, M. A. Akhavan-Behabadi, M. Raisee Dehkordi and S. Delfani, Thermo-optical properties of copper oxide nanofluids for direct absorption of solar radiation, *Sol. Energy Mater. Sol. Cells*, 2016, **144**, 136–142.
- 18 G. Ren, D. Hu, E. W. C. Cheng, M. A. Vargas-Reus, P. Reip and R. P. Allaker, Characterisation of copper oxide nanoparticles for antimicrobial applications, *Int. J. Antimicrob. Agents*, 2009, **33**, 587–590.
- 19 R. Sankar, P. Manikandan, V. Malarvizhi, T. Fathima, K. S. Shivashangari and V. Ravikumar, Green synthesis of colloidal copper oxide nanoparticles using *Carica papaya* and its application in photocatalytic dye degradation, *Spectrochim. Acta, Part A*, 2014, **121**, 746–750.
- 20 S. Anandan, G.-J. Lee and J. J. Wu, Sonochemical synthesis of CuO nanostructures with different morphology, *Ultrason. Sonochem.*, 2012, **19**, 682–686.
- 21 A. El-Trass, H. ElShamy, I. El-Mehasseb and M. El-Kemary, CuO nanoparticles: synthesis, characterization, optical properties and interaction with amino acids, *Appl. Surf. Sci.*, 2012, **258**, 2997–3001.
- 22 S. T. Fardood, A. Ramazani, P. A. Asiabi and S. W. Joo, A novel green synthesis of copper oxide nanoparticles using a henna extract powder, *J. Struct. Chem.*, 2018, **59**, 1737–1743.
- 23 G.-Q. Yuan, H.-F. Jiang, C. Lin and S.-J. Liao, Shape- and size-controlled electrochemical synthesis of cupric oxide nanocrystals, *J. Cryst. Growth*, 2007, **303**, 400–406.
- 24 B. Arunkumar, S. Johnson Jeyakumar and M. Jothibas, A sol-gel approach to the synthesis of CuO nanoparticles using *Lantana camara* leaf extract and their photo catalytic activity, *Optik*, 2019, **183**, 698–705.
- 25 H. Siddiqui, M. R. Parra and F. Z. Haque, Optimization of process parameters and its effect on structure and morphology of CuO nanoparticle synthesized via the sol-gel technique, *J. Sol-Gel Sci. Technol.*, 2018, **87**, 125–135.
- 26 P. P. N. V. Kumar, U. Shameem, P. Kollu, R. L. Kalyani and S. V. N. Pammi, Green synthesis of copper oxide nanoparticles using *Aloe vera* leaf extract and its antibacterial activity against fish bacterial pathogens, *J. Bionanosci.*, 2015, **5**, 135–139.
- 27 M. Nasrollahzadeh, S. M. Sajadi, A. Rostami-Vartooni and S. M. Hussin, Green synthesis of CuO nanoparticles using aqueous extract of *Thymus vulgaris* L. leaves and their catalytic performance for *n*-arylation of indoles and amines, *J. Colloid Interface Sci.*, 2016, **466**, 113–119.
- 28 M. S. Jadhav, S. Kulkarni, P. Raikar, D. A. Barretto, S. K. Vootla and U. S. Raikar, Green biosynthesis of CuO & Ag–CuO nanoparticles from *Malus domestica* leaf extract and evaluation of antibacterial, antioxidant and DNA cleavage activities, *New J. Chem.*, 2018, **42**, 204–213.
- 29 H. Veisi, S. Hemmati and H. Javaheri, N-arylation of indole and aniline by a green synthesized CuO nanoparticles



- mediated by *Thymra spicata* leaves extract as a recyclable and heterogeneous nanocatalyst, *Tetrahedron Lett.*, 2017, **58**, 3155–3159.
- 30 S. Chaudhary, D. Rohilla, A. Umar, N. Kaur and A. Shanavas, Synthesis and characterizations of luminescent copper oxide nanoparticles: toxicological profiling and sensing applications, *Ceram. Int.*, 2019, **45**, 15025–15035.
  - 31 M. Hekmati, Application of biosynthesized CuO nanoparticles using *Rosa canina* fruit extract as a recyclable and heterogeneous nanocatalyst for alkyne/aldehyde/amine A3 coupling reactions, *Catal. Lett.*, 2019, **149**, 2325–2331.
  - 32 S. Phukan, P. Bomjen, T. Shripathi and M. H. Rashid, Green route biosynthesis of shape-tunable ZnO nanostructures and their photocatalytic applications, *ChemistrySelect*, 2017, **2**, 11137–11147.
  - 33 S. Phukan, D. Kakati and M. H. Rashid, Use of invasive weed to synthesize shape-tunable gold nanoparticles and evaluation of their catalytic activities in dye reduction, *Curr. Nanosci.*, 2018, **14**, 511–519.
  - 34 R. Chowdhury, M. M. R. Mollick, Y. Biswas, D. Chattopadhyay and M. H. Rashid, Biogenic synthesis of shape-tunable Au-Pd alloy nanoparticles with enhanced catalytic activities, *J. Alloys Compd.*, 2018, **763**, 399–408.
  - 35 S. Phukan, A. Mahanta, D. Kakati and M. H. Rashid, Green chemical synthesis of Pd nanoparticles for use as efficient catalyst in Suzuki-Miyaura cross-coupling reaction, *Appl. Organomet. Chem.*, 2019, **33**, e4758.
  - 36 J. Gmach, Ł. Joachimiak and K. M. Błażewska, aza-Michael addition of imidazole analogues, *Synthesis*, 2016, **48**, 2681–2704.
  - 37 A. Y. Rulev, aza-Michael reaction: achievements and prospects, *Russ. Chem. Rev.*, 2011, **80**, 197–218.
  - 38 P. Perlmutter, *Conjugate addition reactions in organic synthesis*, Pergamon, 1 edn., 1999.
  - 39 M. J. Bhanushali, N. S. Nandurkar, S. R. Jagtap and B. M. Bhanage,  $\text{Y}(\text{NO}_3)_3 \cdot 6\text{H}_2\text{O}$  catalyzed aza-Michael addition of aromatic/hetero-aromatic amines under solvent-free conditions, *Catal. Commun.*, 2008, **9**, 1189–1195.
  - 40 J. Collin, S. Bezzenine-Lafollée, R. Gil, N. Jaber, M. Martin and I. Reboule, Samarium iodides: catalysts for the formation of carbon-nitrogen bonds, *Synlett*, 2009, **2009**, 2051–2067.
  - 41 K. Damera, K. L. Reddy and G. V. M. Sharma, An efficient  $\text{ZrCl}_4$  catalyzed aza-michael addition reaction: synthesis of C-linked carbo  $\beta$ 3-amino acids, *Lett. Org. Chem.*, 2009, **6**, 151–155.
  - 42 M. K. Chaudhuri, S. Hussain, M. L. Kantam and B. Neelima, Boric acid: a novel and safe catalyst for aza-Michael reactions in water, *Tetrahedron Lett.*, 2005, **46**, 8329–8331.
  - 43 G. A. Ardizzoia, S. Brenna and B. Therrien, Ni(II) and Pd(II) pyridinyloxazolidine-compounds: synthesis, X-ray characterisation and catalytic activities in the aza-Michael reaction, *Dalton Trans.*, 2012, **41**, 783–790.
  - 44 X. Chen, X. Li, H. Song, Y. Qian and F. Wang, Solvent-free aza-Markovnikov and aza-Michael additions promoted by a catalytic amount of imidazolide basic ionic liquids, *Tetrahedron Lett.*, 2011, **52**, 3588–3591.
  - 45 J.-M. Xu, Q. Wu, Q.-Y. Zhang, F. Zhang and X.-F. Lin, A basic ionic liquid as catalyst and reaction medium: a rapid and simple procedure for aza-Michael addition reactions, *Eur. J. Org. Chem.*, 2007, **2007**, 1798–1802.
  - 46 L. Li, Z. Liu, Q. Ling and X. Xing, Polystyrene-supported CuI-imidazole complex catalyst for aza-Michael reaction of imidazoles with  $\alpha,\beta$ -unsaturated compounds, *J. Mol. Catal. A: Chem.*, 2012, **353–354**, 178–184.
  - 47 L. T. L. Nguyen, T. T. Nguyen, K. D. Nguyen and N. T. S. Phan, Metal-organic framework MOF-199 as an efficient heterogeneous catalyst for the aza-Michael reaction, *Appl. Catal., A*, 2012, **425–426**, 44–52.
  - 48 L. Dai, Y. Zhang, Q. Dou, X. Wang and Y. Chen, Chemo/regioselective aza-Michael additions of amines to conjugate alkenes catalyzed by polystyrene-supported  $\text{AlCl}_3$ , *Tetrahedron*, 2013, **69**, 1712–1716.
  - 49 S. Jammi, S. Sakthivel, L. Rout, T. Mukherjee, S. Mandal, R. Mitra, P. Saha and T. Punniyamurthy, CuO nanoparticles catalyzed C–N, CO, and C–S cross-coupling reactions: scope and mechanism, *J. Org. Chem.*, 2009, **74**, 1971–1976.
  - 50 M. Tajbakhsh, M. Farhang and A. A. Hosseini, MgO nanoparticles as an efficient and reusable catalyst for aza-Michael reaction, *J. Iran. Chem. Soc.*, 2014, **11**, 665–672.
  - 51 Z.-X. Li, D. Luo, M.-M. Li, X.-F. Xing, Z.-Z. Ma and H. Xu, Recyclable  $\text{Fe}_3\text{O}_4$  nanoparticles catalysts for aza-Michael addition of acryl amides by magnetic field, *Catalysts*, 2017, **7**, 219.
  - 52 R. Chowdhury, N. Barah and M. H. Rashid, Facile biopolymer assisted synthesis of hollow  $\text{SnO}_2$  nanostructures and their application in dye removal, *ChemistrySelect*, 2016, **1**, 4682–4689.
  - 53 A. S. Ethiraj and D. J. Kang, Synthesis and characterization of CuO nanowires by a simple wet chemical method, *Nanoscale Res. Lett.*, 2012, **7**, 70.
  - 54 R. A. Zarate, F. Hevia, S. Fuentes, V. M. Fuenzalida and A. Zúñiga, Novel route to synthesize CuO nanoplatelets, *J. Solid State Chem.*, 2007, **180**, 1464–1469.
  - 55 K. S. W. Sing, D. H. Everett, R. A. W. Haul, L. Moscou, R. A. Pierotti, J. Rouquerol and T. Siemieniowska, Reporting physisorption data for gas/solid systems with special reference to the determination of surface area and porosity, *Pure Appl. Chem.*, 1985, **57**, 603–619.

